

# Structural insight into hormone recognition by the natriuretic peptide receptor-A

Haruo Ogawa<sup>1</sup>  and Masami Kodama<sup>2</sup>

<sup>1</sup> Department of Structural Biology, Graduate School of Pharmaceutical Sciences, Kyoto University, Japan

<sup>2</sup> Department of Bio-informational Pharmacology, School of Pharmaceutical Sciences, University of Shizuoka, Japan

## Keywords

atrial natriuretic peptide; crystal structure; hormone recognition; natriuretic peptide; natriuretic peptide receptor-A

## Correspondence

H. Ogawa, Graduate School of Pharmaceutical Sciences, Kyoto University, 46-29 Yoshida Shimoadachi-cho, Sakyo-ku, Kyoto 606-8501, Japan  
 Tel: +81 75 753-4606  
 E-mail: [haru@pharm.kyoto-u.ac.jp](mailto:haru@pharm.kyoto-u.ac.jp)

(Received 19 June 2023, revised 21 November 2023, accepted 16 February 2024)

doi:10.1111/febs.17104

Atrial natriuretic peptide (ANP) plays a central role in the regulation of blood pressure and volume. ANP activities are mediated by natriuretic peptide receptor-A (NPR-A), a single-pass transmembrane receptor harboring intrinsic guanylate cyclase activity. This study investigated the mechanism underlying NPR-A-dependent hormone recognition through the determination of the crystal structures of the NPR-A extracellular hormone-binding domain complexed with full-length ANP, truncated mutants of ANP, and dendroaspis natriuretic peptide (DNP) isolated from the venom of the green Mamba snake, *Dendroaspis angusticeps*. The bound peptides possessed pseudo-two-fold symmetry, despite the lack of two-fold symmetry in the primary sequences, which enabled the tight coupling of the peptide to the receptor, and evidently contributes to guanylyl cyclase activity. The binding of DNP to the NPR-A was essentially identical to that of ANP; however, the affinity of DNP for NPR-A was higher than that of ANP owing to the additional interactions between distinctive sequences in the DNP and NPR-A. Consequently, our findings provide valuable insights that can be applied to the development of novel agonists for the treatment of various human diseases.

## Introduction

The cardiac hormone, atrial natriuretic peptide (ANP) [1], is produced in the cardiac atria and secreted into the circulatory system in response to volume expansion and increased atrial distension. ANP has potent natriuretic, diuretic, vasodilator, and renin- and aldosterone-suppressing activities, and assumes a pivotal role in the regulation of blood pressure and volume [2–4]. ANP is a cyclic peptide comprising 28 amino acid residues [5] and belongs to the natriuretic peptide family, which includes B-type (BNP) [6], and C-type (CNP) [7] natriuretic peptides. The activities of ANP and BNP resemble each other [8], whereas CNP apparently contributes

to the central nervous system-mediated control of blood pressure and salt-fluid balance [8,9], cartilage homeostasis, and endochondral bone formation [10]. Dendroaspis natriuretic peptide (DNP) is a protein that has recently been isolated from the venom of the green Mamba, *Dendroaspis angusticeps* [11].

Dendroaspis natriuretic peptide is a potent natriuretic and diuretic peptide, is similar to ANP and BNP, and induces an elevation in urinary and plasma cGMP levels [12,13]. The affinity of DNP for NPR-A is reported to be higher than that of ANP and BNP [14]. Compared to ANP, BNP, and CNP, DNP flaunts

## Abbreviations

ANP, atrial natriuretic peptide; BNP, B-type natriuretic peptide; BN-PAGE, blue native polyacrylamide gel electrophoresis; cGMP, cyclic guanosine monophosphate; CNP, C-type natriuretic peptide; DNP, dendroaspis natriuretic peptide; ECD, extracellular domain; GCase, guanylate cyclase; hANP, human atrial natriuretic peptide; hCNP, human C-type natriuretic peptide; MD, membrane distal; MP, membrane proximal; NPR-A, A-type natriuretic peptide receptor; NPR-B, B-type natriuretic peptide receptor; rANP, rat atrial natriuretic peptide; rBNP, rat B-type natriuretic peptide.

elongated N- and C-termini and is more stable against neutral endopeptidase [15], which is the primary inactivator of natriuretic peptides. Based on the enhanced stability and high potency of DNP, chimeras of DNP and other natriuretic peptides have been created and assessed in clinical trials for the remediation of heart failure [16,17]. Therefore, a comprehensive elucidation pertaining to the differences between the binding of ANP and DNP to NPR-A is essential for future drug discovery and research focused on therapeutic strategies for heart failure.

The activities of ANP and BNP are mediated by the natriuretic peptide receptor-A (NPR-A), a single-pass transmembrane receptor harboring intrinsic guanylate cyclase (GCase) activity [18]. The NPR-A consists of a glycosylated extracellular hormone-binding domain and an intracellular domain that includes protein kinase-like and GCase catalytic domains and acts as a homodimer. The closely related B-type natriuretic peptide receptor (NPR-B) mediates the activities of CNP [9]. NPR-A and NPR-B belong to a family of GCase-coupled receptors that share a similar overall molecular configuration [19,20], and they may also share a common signal transmission mechanism upon ligand binding. Nonetheless, the mechanism underlying NPR-A- and NPR-B-mediated recognition of natriuretic peptides possessing near-identical sequences remains unknown.

The crystal structure of the NPR-A extracellular ANP-binding domain (NPR-A<sub>ECD</sub>) complexed with a rat partial ANP comprising amino acids 7–27 (rANP [7–27]) [21] was determined to investigate the ligand recognition and transmembrane signaling mechanisms mediated by NPR-A. One molecule of bound ANP was observed to be flanked by two NPR-A monomers. Compared with the *apo* structure [22], NPR-A induced rotational motion with no appreciable intramolecular modification in either of the monomers [21]. However, the relatively low resolution of the previous datasets [21] and the existence of the bound ANP in two alternative conformations (orientations) of equal occupancy (50%) related by a two-fold symmetry, which rendered the assignment of the bound ANP complicated. Consequently, the mechanism underlying the receptor-dependent ligand recognition remained ambiguous.

Therefore, this study aimed at determining the high-resolution crystal structures of NPR-A in complexes with rat and human full-length ANP, DNP, and various ANP mutants. This study advances research pertaining to this topic and addresses knowledge gaps, including ligand recognition mechanisms associated with NPR-A. The knowledge gleaned from our study can be potentially extended to other related receptors, applied to drug discovery and design, and facilitate

further expansion of research on the treatment of heart failure.

## Results

### Determination of the structure and precise model building of the bound natriuretic peptides

The extracellular domain of NPR-A<sub>ECD</sub>, comprising amino acid residues 1–435, was expressed and purified as previously described [21,23,24]. All structures (Table 1, Fig. 1A) were solved by molecular replacement using the *apo* structure (PDB accession code 1DP4 [22]) as the template. The resolution of the newly determined structures displayed substantial enhancements (Table 1) compared to the previously determined structure [21]. Consequently, the current electron density maps portrayed drastic improvement in comparison to the previously determined map (Fig. 1B–D, Fig. S1A–D). The electron density corresponding to the side chains of the bound peptides was barely discernible in the previous electron density map but was evident in the new map (Fig. S1A). Furthermore, an electron density map of DNP was generated, which depicted the presence of the side chains (Fig. S2A). Nonetheless, although the new maps were apparent improvements over the previous map, several discrepancies were noted between the new maps and previously determined substrate structure (rANP [7–27]). The structure of rANP [7–27] [21] could be roughly fitted with the new rANP [1–28] map (Fig. S1D). Conversely, DNP constructed by replacing the side chains of ANP with those of DNP did not adhere to its electron density map at all (Fig. S2B). Particularly, neither was there any density covering the main and side chains of Lys11, nor any side chain filling the inner density of the ring structure of DNP. This evidence means that the path of the ANP main chain in the ring structure should be completely revised to correctly model the DNP. However, given the very similar electron density maps of the ring structures of ANP and DNP (Fig. 1B–D, Figs S1A and S2A) and the similarity of their sequences (Fig. 1A), the main chain pathways of ANP and DNP should be similar. Therefore, the previous map [21] had limitations in terms of accurate modeling due to its low resolution (Fig. S1A). Although it was derived from our best possible interpretation, we concluded that we needed to modify and revise the previous model.

Modeling the bound peptides was highly challenging. While the bound peptides had no internal symmetry in the primary sequence (Fig. 1A), the calculated electron density maps showed obvious two-fold symmetry (Fig. 1B–D). These findings indicate that the two

**Table 1.** Data collection and refinement statistics.

Data collection	rANP [1–28]	hANP [1–28]	DNP
Space group	$P6_1$	$P6_1$	$P6_1$
No. crystals	2	2	2
Cell dimensions			
<i>a</i> , <i>b</i> , <i>c</i> (Å)	100.2, 100.2, 261.9	100.2, 100.2, 261.7	99.6, 99.6, 262.5
Resolution (Å)	50.0–2.45 (2.52–2.45) <sup>a</sup>	50.0–2.45 (2.52–2.45) <sup>a</sup>	50.0–2.45 (2.52–2.45) <sup>a</sup>
$R_{\text{merge}}$	6.0 (35.5)	4.0 (36.7)	5.3 (25.5)
$I/s$	30.5 (2.6)	34.9 (3.2)	30.0 (4.6)
$CC_{1/2}$	0.99 (0.56)	0.99 (0.51)	0.99 (0.66)
Completeness (%)	99.6 (98.8)	96.8 (98.1)	96.3 (99.5)
Redundancy	22.3 (19.5)	27.8 (19.8)	22.1 (16.5)
Refinement			
Resolution (Å)	32.9–2.45 (2.53–2.45)	43.5–2.45 (2.53–2.45)	30.7–2.45 (2.53–2.45)
No. reflections	52 690 (4850)	52 727 (4831)	51 983 (4880)
$R_{\text{work}}/R_{\text{free}}$	0.193/0.249 (0.306/0.314)	0.205/0.259 (0.305/0.335)	0.201/0.241 (0.290/0.312)
No. atoms			
Protein	6944	6944	6944
Ligand	189	189	231
Waters, ions	135	133	127
<i>B</i> -factors			
Protein	89.9	86.1	63.3
Ligand	86.4	80.9	58.0
Waters, ions	68.3	64.4	42.3
R.m.s deviations			
Bond lengths (Å)	0.006	0.009	0.006
Bond angles (°)	0.785	0.994	0.829

Data collection	hANP [7–28]	hANP [5–27]
Space group	$P6_1$	$P6_1$
No. crystals	2	2
Cell dimensions		
<i>a</i> , <i>b</i> , <i>c</i> (Å)	99.8, 99.8, 260.4	99.4, 99.4, 259.7
Resolution (Å)	50.0–2.7 (2.78–2.70) <sup>a</sup>	50.0–2.85 (2.93–2.85) <sup>a</sup>
$R_{\text{merge}}$	3.1 (30.7)	7.8 (24.3)
$I/s$	23.5 (3.5)	26.4 (5.3)
$CC_{1/2}$	0.99 (0.53)	0.99 (0.55)
Completeness (%)	99.3 (99.5)	90.2 (99.9)
Redundancy	10.9 (9.6)	15.4 (7.3)
Refinement		
Resolution (Å)	43.3–2.70 (2.81–2.70)	43.1–2.85 (3.03–2.85)
No. reflections	39 898 (4415)	30 550 (5626)
$R_{\text{work}}/R_{\text{free}}$	0.190/0.234 (0.314/0.370)	0.173/0.230 (0.267/0.312)
No. atoms		
Protein	6944	6944
Ligand	166	166
Waters, ions	131	103
<i>B</i> -factors		
Protein	89.1	91.8
Ligand	101.1	91.2
Waters, ions	65.6	68.8
R.m.s deviations		
Bond lengths (Å)	0.009	0.008
Bond angles (°)	0.989	0.965

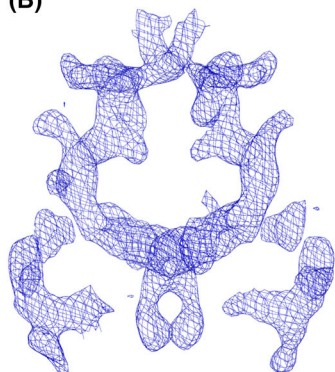
<sup>a</sup>Highest resolution shell is shown in parenthesis.

(A)

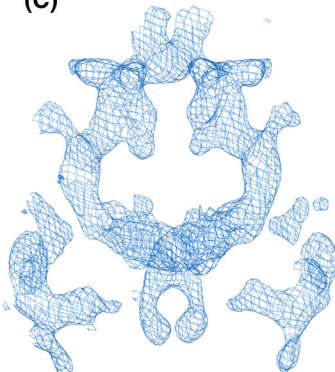
```

rANP [1-28] : SLRRSSCFGGRIDRIGAQSGLG CNSFRY
rANP [4-17, 23] : RSSCFGGRIDRI-----C
hANP [1-28] : SLRRSSCFGGRMDRIGAQSGLG CNSFRY
hANP [7-28] : CFFGGRMDRIGAQSGLG CNSFRY
hANP [5-27] : SSSCFGGRMDRIGAQSGLG CNSFR
DNP : EVKYDPCFEGHKIDRINHVSNLGCPSLRDPRPNAPSTSA
hBNP : SPKMQVQSGCFGRKMDRISSSSGLGCKVLRRH
hCNP : GLSKGCFGLKIDRIGSMSGLGC
    
```

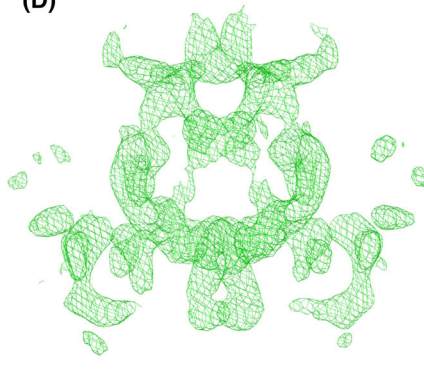
(B)



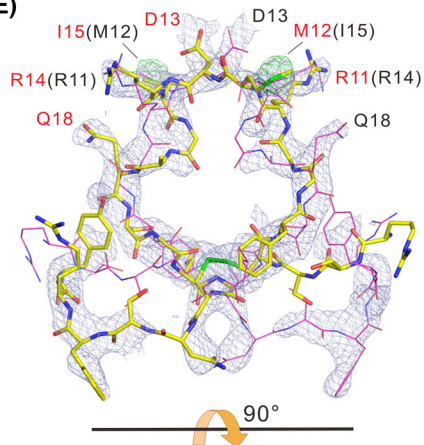
(C)



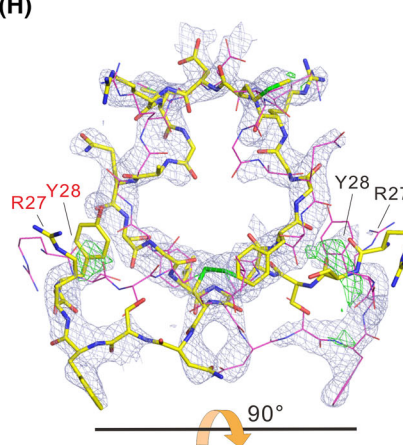
(D)



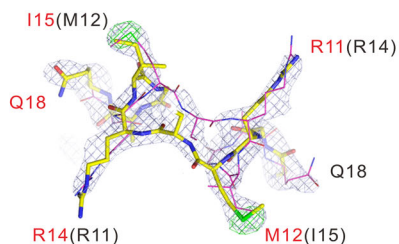
(E)



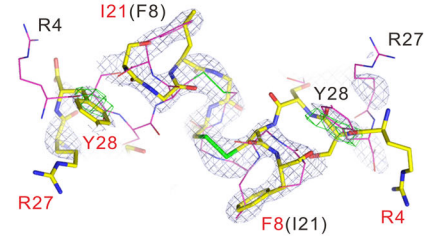
(H)



(F)



(I)



(G)

```

hANP [1-28] - rANP [1-28]
hANP [1-28] : SLRRSSCFGGRMDRIGAQSGGLGCNSFRY
-rANP [1-28] : SLRRSSCFGGRIDRIGAQSGGLGCNSFRY
-----
M
    
```

(J)

```

hANP [1-28] - hANP [5-27]
hANP [1-28] : SLRRSSCFGGRMDRIGAQSGGLGCNSFRY
-hANP [5-27] : SSSCFGGRMDRIGAQSGGLGCNSFR
-----
SLRR Y
    
```

**Fig. 1.** Electron density maps around the peptides. (A) Sequence alignment of natriuretic peptides used in this work. Two Cys residues (blue with underscore) form an SS-bond, and the peptide forms a cyclic structure. Amino acid residues masked with yellow have conserved sequences between natriuretic peptides. Amino acid residues shown in green and red are hANP- and DNP-specific, respectively. UniProt accession numbers for rANP [1–28] and rANP [4–17.23] is P01161, for hANP [1–28], hANP [7–28], and hANP [5–27] is P01160, for DNP is P28374, for hBNP is P16860, and for hCNP is P23582. (B–D) Initial electron density maps around (B) rANP [1–28], (C) hANP [1–28], and (D) DNP contour level at  $2.5\sigma$ . (E–J)  $|F_{\text{obs(peptide1)}}| - |F_{\text{obs(peptide2)}}|$  maps between multiple ligand complexes. (E–G)  $|F_{\text{obs(hANP [1–28])}}| - |F_{\text{obs(rANP [1–28])}}|$  map at  $12.5\sigma$ . The map clearly shows the sulfur atom of Met12 in hANP [1–28]. (H–J)  $|F_{\text{obs(rANP [1–28])}}| - |F_{\text{obs(rANP [5–27])}}|$  map at  $5.0\sigma$ . The map clearly shows the locations of Tyr28. Since two ANP molecules are comprised of two ligand molecules having two alternative conformations (orientations) with two-fold symmetry at their binding sites with an occupancy of 50%, one conformation is shown as a yellow stick and the other is shown as a thin purple stick. All structure figures were prepared using PYMOL 2.4.0a (The PyMOL Molecular Graphics System, <http://www.pymol.org>). All amino acid sequence alignments (A, G, J) were performed manually.

natriuretic peptides have two alternative conformations (orientations) with two-fold symmetry at their binding sites with an occupancy of 50% (Fig. 1B–D). In fact, electron density for the characteristic side chains in the ANP was almost lost in the previous map due to low resolution (Fig. S1A). In addition, only the bound structure of the bound rANP [7–27] was determined, and no comparison with other substrates was performed in the previous study [21]. In this study, by using new high-resolution maps, we calculated a series of  $|F_{\text{obs(peptide1)}}| - |F_{\text{obs(peptide2)}}|$  electron density maps between multiple ligand complexes to illuminate differences in the specific amino acid sequences (Fig. 1E–J). For example, the amino acids differ between human and rat ANP only at position 12, being Met in humans but Ile in rats (Fig. 1A). Because a sulfur atom located at the tip of the Met side chain has a larger electron density than the carbon atom in Ile, the electron density derived from a sulfur atom of Met12 was expected in the calculated  $|F_{\text{obs(hANP [1–28])}}| - |F_{\text{obs(rANP [1–28])}}|$  map. Indeed, the  $|F_{\text{obs(hANP [1–28])}}| - |F_{\text{obs(rANP [1–28])}}|$  map at  $12\sigma$  clearly shows the sulfur site of Met12 in the hANP (or Ile12 in the rANP [1–28]) in the two alternative conformations (Fig. 1E,F). This calculation is possible because the unit cell dimensions of the crystals are essentially the same (Table 1). This strategy was also useful for the truncated ANPs or the other natriuretic peptides, such as DNP, unless there is a significant difference in the unit cell dimensions between the crystals. The  $|F_{\text{obs(rANP [1–28])}}| - |F_{\text{obs(rANP [5–27])}}|$  map at  $5\sigma$  shows the locations of Tyr28 in the two conformations (Fig. 1H,I). By defining the locations of specific side chains using this strategy, 11 residues, each in ANP and DNP were identified. Under the guidance of multiple difference density maps of different peptides, we successfully modeled amino acid residues 4–28 of hANP [1–28] or rANP [1–28], and amino acid residues 1–28 of DNP with no ambiguity (Fig. 1E–J, Figs S3 and S4).

The revised model of the ANP fitted well with the new map (Fig. 1E–I, Figs S1 and S3). The model differed from the previously modeled structure in many aspects,

including the pathway of the main chain and the locations of the side chains, except for the approximate positions of Cys7, Phe8, Leu21, and Cys23 (Fig. S1B–D). In many respects, however, the revised model was reasonable compared to the previous one. For example, in the previous model, Arg11 protruded far outside the ring structure of the ANP and the electron density was barely visible in the previous map (Fig. S1A,B), but in the new map, R11 was located within the appropriate density (Fig. S1C). Almost all the other side chains were located within the appropriate density in the new map (Fig. S1C). The newly constructed DNP also fitted well with the map (Figs S2C and S4). Lys11, which had no density in the previous ANP-based structure for DNP (Fig. S2B), was now placed within the appropriate density (Fig. S2C). Also, the inner density of the ring structure, which did not contain any main or side chains, was now filled with the side chains derived from Asn16 and His17 (Fig. S2C). The overall shape of the main chain of the ANP and DNP was similar (Fig. 3, Figs S1 and S2), indicating that they shared the same skeletal features as natriuretic peptides. On the other hand, there were many side chains protruding from DNP that were not conserved in ANP (Figs 1A and 3D). Since these side chains are characteristic of DNP and not present in ANP (Fig. 1A), they are presumed to be the key to the characteristic function of DNP.

The revised model of the rANP [1–28] also fits well with the previous low-resolution map (Fig. S1D). We also refined the revised model of the NPR-A<sub>ECD</sub> with the newly modeled ANP against the previous structure factor [21]. The calculated  $R$ -factors were lower when the revised model was used ( $R_{\text{work}}/R_{\text{free}}$ , 20.2/27.4) than when the previous model was used as the initial model ( $R_{\text{work}}/R_{\text{free}}$ , 22.3/28.3). This evidence suggests that the revised model is more reasonable than the previous one.

## Overall structures

The overall structures and enlarged views around ligand-binding sites of NPR-A<sub>ECD</sub> with bound full-

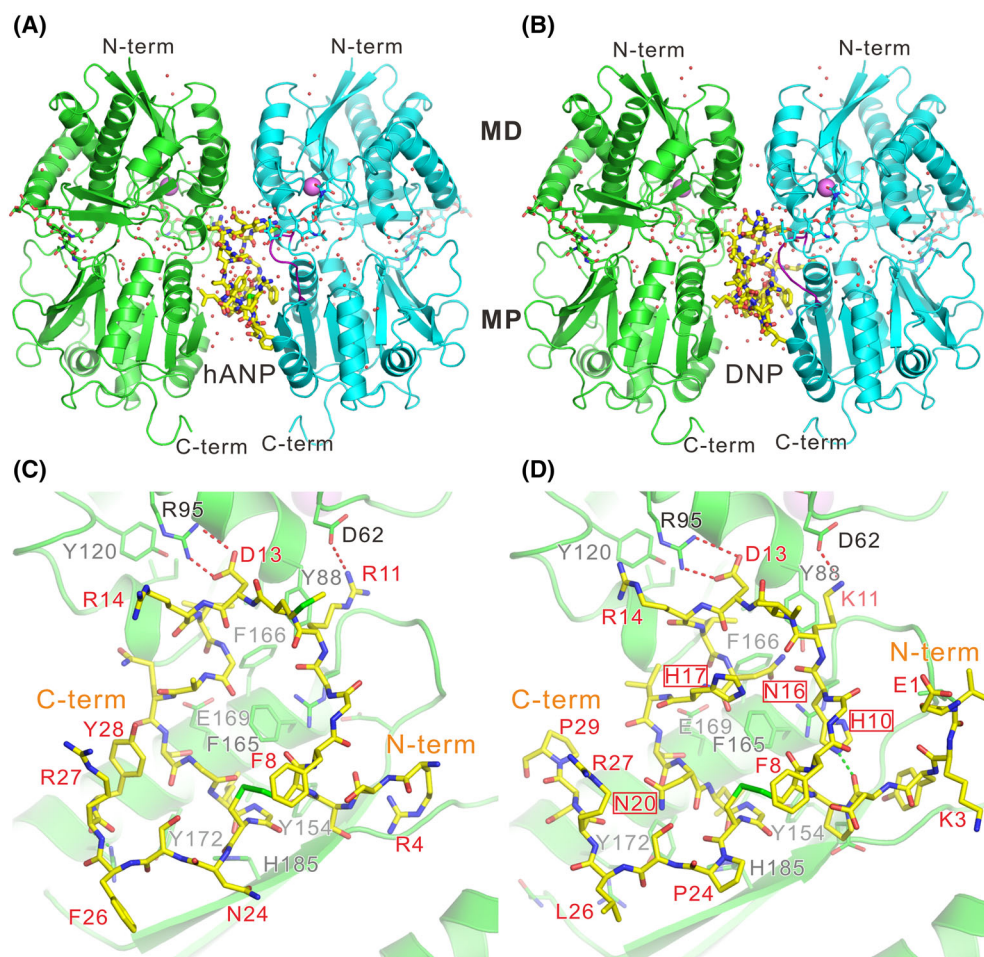


**Fig. 2.** Structures of NPR-A with bound natriuretic peptides. (A, B) Overall structures of NPR-A with bound hANP [1–28] (A) and DNP (B). NPR-A is represented as a ribbon model in which monomers A and B are shown in green and cyan, respectively. Bound ligands are shown as yellow sticks. The receptor monomer consists of two globular domains, a membrane distal (MD) domain, and a membrane proximal (MP) domain. Red, oxygen; blue, nitrogen; yellow-green, sulfite atoms. Water molecules are shown as red spheres. (C, D) Magnified views around bound hANP [1–28] (C) and DNP (D), looking from monomer A. (D) Amino acids surrounded by red squares are DNP-specific residues. All structure figures were prepared using PYMOL 2.4.0a (The PyMOL Molecular Graphics System, <http://www.pymol.org>).

length human ANP (hANP [1–28]) and dendroaspis natriuretic peptide (DNP) are shown (Fig. 2). ANP and DNP are cyclic peptides with a disulfide bond between Cys7 and Cys23 (Fig. 1A). The bound peptides are sandwiched between two monomers of NPR-A<sub>ECD</sub> with two-fold symmetry, which is similar to our previous findings of the structure in complex with rANP [7–27] [21]. The receptor monomer consists of two globular domains, a membrane distal (MD) domain, and a membrane proximal (MP) domain. One Cl<sup>-</sup> ion, which is indispensable for ANP binding to NPR-A, is bound to the MD domain [25,26] and two sugar modifications are located at Asn13 and Asn395 in the MD and MP domains, respectively. The structure contains many water molecules, including the ligand-binding site

(Fig. 2A,B). The structures of NPR-A<sub>ECD</sub> with bound ANP and DNP are almost identical except for one loop connecting the MD and MP domains (Fig. 2). Other than hANP [1–28] and DNP, we determined the structures of NPR-A<sub>ECD</sub> complexed with full-length rat ANP (rANP [1–28]), truncated mutants of hANP (Fig. 1A, Figs S3 and S5, Table 1).

### The ring structure of natriuretic peptides

The ring structure of the bound natriuretic peptides (amino acid residues from Cys7 to Cys23) exhibited pseudo-two-fold symmetry (Fig. 3), which is not a feature of the primary sequences of natriuretic peptides (Fig. 1A). This symmetry was not observed in the

previously reported structure (Fig. S1A). One region with two-fold symmetry was located at the top of the ring structure (Fig. 3A,B,D,E,G). In the case of hANP, positively charged residues (Arg11 and Arg14) and nonpolar amino acid residues (Met12 and Ile15) were positioned with pseudo-two-fold symmetry, centered on Asp13 at the top of the ring structures (Fig. 3B). Although there is a replacement of Arg11 with Lys11 in DNP and a replacement of Met12 with Ile12 in DNP or rANP, this scenario is essentially similar in the NPR-A<sub>ECD</sub> with bound DNP (Fig. 3D,E) or rANP [1–28] (Fig. S6A,B). These positively charged residues and nonpolar residues possessing pseudo-two-fold symmetry well fitted into symmetrical hydrophilic pockets in the NPR-A composed of Asp62, Glu119, and carbonyl oxygen atom of Asp160, and hydrophobic pockets in the NPR-A composed of Tyr88, Ala111, Ile114, Tyr120, and Phe166, respectively (Fig. 3H). Thereby, the binding of peptides to the NPR-A becomes stable. The other region with two-fold symmetry in the ring structure was located at the bottom centered on the SS-bond between Cys7 and Cys23 (Fig. 3A,C,D,F,G). In the case of hANP, nonpolar amino acid residues (Phe8 and Leu21) are positioned with pseudo-two-fold symmetry (Fig. 3A,C). Again, this scenario is essentially the same in the NPR-A<sub>ECD</sub> with bound DNP (Fig. 3D,F) or rANP [1–28] (Fig. S4A,C). Both nonpolar residues are firmly embedded in the hydrophobic pocket in the NPR-A composed of Tyr154, Phe165, Tyr172, and His185, thus stabilizing peptide binding to the NPR-A (Fig. 3I).

### The architecture of the ligand recognition by NPR-A

For the comparison with DNP, we used the structure of hANP [1–28] as the standard, because the structures of the bound hANP [1–28] and rANP [1–28] are essentially identical except for amino acid residue 12. We found that four common features in ANP and DNP are essential for their binding to NPR-A. One is the pseudo-two-fold symmetry at the top of the ring structure, consisting of positively charged residues and nonpolar residues centered on Asp13(ANP) (Fig. 3A,B,D,E,H, Fig. S6A,B). The second is the pseudo-two-fold symmetry at the bottom of the ring structures consisting of Phe8 and Leu21 centered on the SS-bond (Fig. 3A,C,D,F,I, Fig. S6A,C). The third is Asp13 (ANP) at the center of the pseudo-two-fold symmetry at the top of the ring structure, positioned at the boundary between monomers A and B of the NPR-A and forming a tight salt bridge with Arg95(A), which played a key role in mediating between monomers A and B through Glu119(A), Tyr120(B), and Asp62 (B)

(Figs 2C,D and 3B,E). The fourth feature is a pseudo- $\beta$ -sheet between 3 amino acid residues immediately after the SS-bond of the ring structure (amino acid residues 24–26) and monomer B of the NPR-A (Fig. 4A,E). The essential feature of this pseudo- $\beta$ -sheet was shown to be common to both ANP and DNP (Fig. 4A,E). The carbonyl oxygen atom of Asn24(ANP) or Pro24(DNP) was shown to form a hydrogen bond with the nitrogen atoms of Glu187(B), and the nitrogen atom of Phe26(ANP) or Leu26(DNP) was shown to form a hydrogen bond with the carbonyl oxygen atom of Glu187(B) (Fig. 4A,E). Ser25 in ANP or DNP formed a hydrogen bond with Glu187(B) (Fig. 4A,E). The residues used for hydrogen bonding in ANP and DNP slightly differed due to the difference in the amino acid residues between them. In ANP, Asn24(ANP) formed a hydrogen bond with the carbonyl oxygen of His185(B), whereas, in DNP, the carbonyl oxygen of Leu26(DNP) formed a hydrogen bond with His195(B) (Fig. 4A,E).

The N-terminal sequences in ANP and DNP are completely different (Fig. 1A), and as a result, the direction of the main chain in each peptide was quite different (Fig. 4B,F). The N-terminus of DNP was well resolved, and they had a tight interaction with NPR-A through three hydrogen bonds formed between Glu1(DNP)-Arg174(B), Lys3(DNP)-Asn180 (B), and Asp5(DNP)-Tyr172(B) (Fig. 4F). Conversely, the N-terminus of ANP was not well resolved. Although an internal hydrogen bond in ANP formed between Arg4(ANP) and Ser6(ANP) was observed, no interaction with NPR-A was detected (Fig. 4B). Although the C-terminal sequence in ANP and DNP is completely different (Fig. 1A), the C-termini of both ANP and DNP seemed to play important roles in interactions with NPR-A in different ways (Fig. 4C, G). The C-terminal residue Tyr28 in ANP played an important role in the formation of the tight NPR-A/ANP complex, as its carboxyl-terminal oxygen atom formed a hydrogen bond with Arg176(A) (Fig. 4C). In addition, the side chain of Tyr28(ANP) formed a hydrogen bond with the carbonyl oxygen atom of Ala17(ANP), stabilizing the ring structure of ANP (Fig. 4C). In the case of DNP, induced fit to DNP occurred in NPR-A, which was never observed in NPR-A in complex with ANP (Fig. 4C,G, Fig. S5). A loop composed of 155–161 of the monomer B came close to Arg27(DNP) (Fig. 4G, Fig. S5). As a result, Asp156(B) in the loop contributed to forming additional hydrogen bonds with Asp156(B) and Arg162(B) (Fig. 4G). No specific bond was detected between NPR-A and Asp28(DNP) or Pro29(DNP), and amino acid residues after 30 were not well resolved in DNP.

The most characteristic difference between ANP and DNP was seen in the four DNP-specific amino acid residues (His10, Asn16, His17, and Asn20) within the ring structure of the peptides (Fig. 1A), wherein the corresponding residues in ANP were all Gly or Ala (Gly10, Gly16, Ala17, and Gly20) (Fig. 1A). His10(DNP) formed a hydrogen bond with the carbonyl oxygen of Asp5(DNP), and the direction of the His-ring of His10(DNP) was fixed in DNP (Fig. 4H). As a result, His10(DNP) constituted a stack of  $\pi$

interactions between Arg162(A) and Phe165(A). Asn16 (DNP) formed a hydrogen bond between the carbonyl oxygen atoms of His10(DNP), Tyr88(A), and Arg162 (A) (Fig. 4H). Although water molecules surrounded the corresponding residues Gly10 and Gly16 in ANP, no direct hydrogen bond between ANP and the NPR-A was evident around these residues (Fig. 4D).

Taken together, it is evident that DNP formed more interactions with NPR-A than that formed with ANP. It is reported that the affinity of DNP for the NPR-A

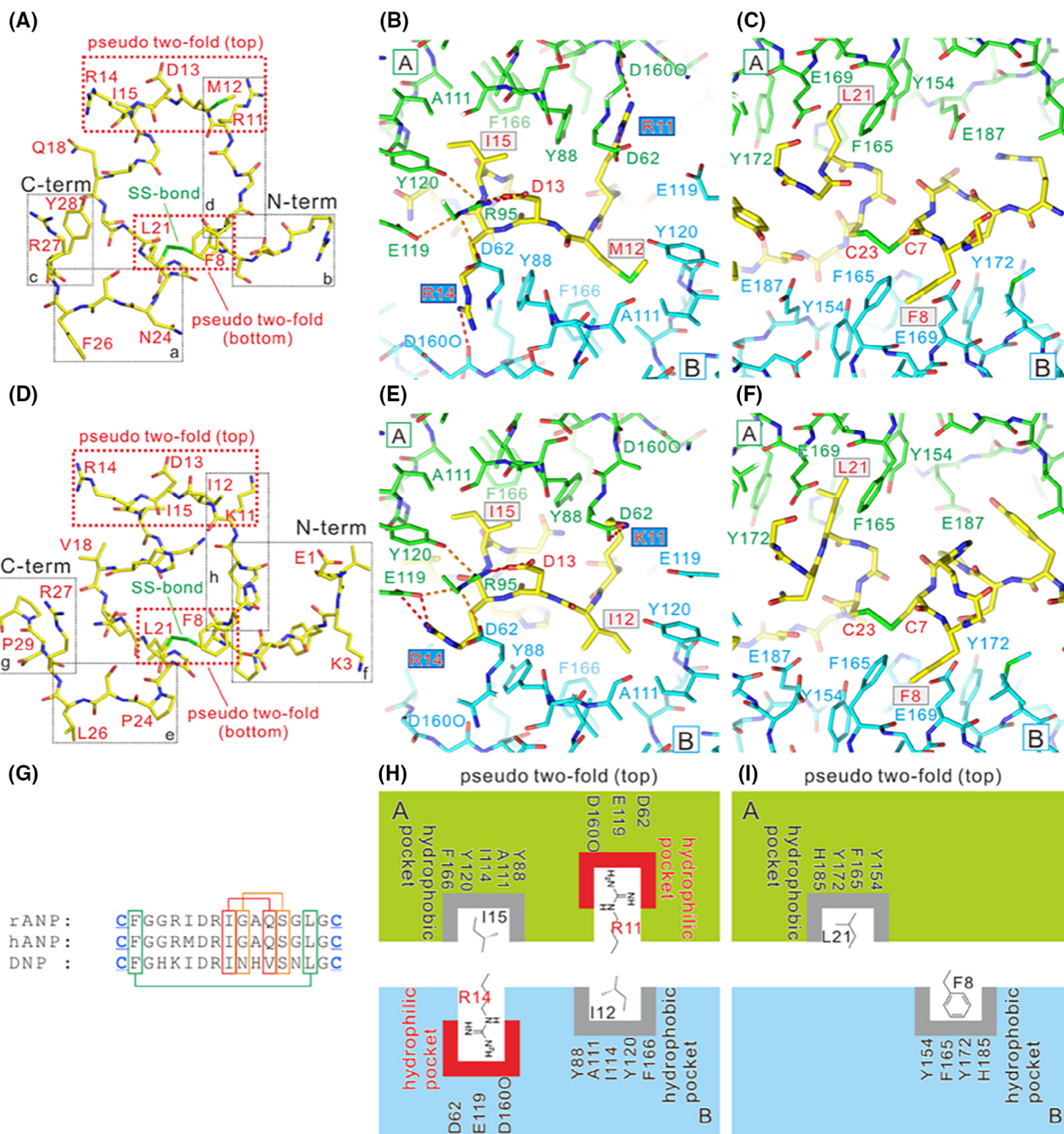


**Fig. 3.** Pseudo-two-fold symmetry in the bound peptides. (A–C) The structure of hANP [1–28] and (D–F) DNP bound to the NPR-A. hANP [1–28] and DNP have pseudo-two-fold symmetry at the top and bottom of ring structures surrounded by red dotted boxes (A, D). The regions surrounded by black dotted boxes with alphabets a–d (A) and with alphabets e–h (D) are the regions used for the magnified views in Fig. 4. (B, C, E, F) Magnified views of pseudo-two-fold symmetry region at the top of the rings in hANP [1–28] (B) and DNP (E). One consists of positively charged residues (Arg11 and Arg14 (hANP [1–28]) or Lys11 and Arg14(DNP)). The other one consists of nonpolar residues (Met12 and Ile15 (hANP [1–28]) or Ile12 and Ile15(DNP)). Magnified views of pseudo-two-fold symmetry region at the bottom of rings in hANP [1–28] (C) and DNP (F). Hydrophobic pairs of Phe8 and Leu21 centered on the disulfide bond composed of Cys7 and Cys23 have pseudo-two-fold symmetry. Hydrophobic pairs can enter the symmetrical hydrophobic pocket of NPR-A monomers. All molecules are represented as sticks. Monomers A and B are green and cyan, respectively. The bound ligands are shown as yellow sticks. Red, oxygen; blue, nitrogen; yellow-green, sulfite atoms. Red dashed lines represent hydrogen bonds. Two independent pairs with pseudo-two-fold symmetry at the top of each ring structure are centered on Asp13. All structure figs (A–F) were prepared using PYMOL 2.4.0a (The PyMOL Molecular Graphics System, <http://www.pymol.org>). (G) Sequence alignment in the ring structure of the natriuretic peptides determined in this study. Residues that contribute to forming pseudo-two-fold symmetry in the tertiary structure are boxed and linked with lines. Uniprot accession number for rANP is P01161, for hANP is P01160, and for DNP is P28374. (H) Mechanism by which rANP with pseudo-two-fold symmetry in the top region can bind to the homodimer of NPR-A. (I) The mechanism by which rANP with pseudo-two-fold symmetry can bind to the homodimer of NPR-A in the bottom region.

is stronger than that of ANP [14]. Our findings supported that DNP has a higher affinity to the NPR-A than ANP.

### Identification of key residues in ANP involved in NPR-A binding

We further investigated the details of substrate binding to the NPR-A using blue native polyacrylamide gel electrophoresis (BN-PAGE). We detected a band for NPR-A without a ligand in the region of NPR-A monomer, but the band for the NPR-A complexed with physiological ligands (hANP [1–28], rANP [1–28], rBNP, or DNP) resolved at the region of the dimer in NPR-A (Fig. 5, Fig. S7). In contrast, when CNP, which is not a ligand for NPR-A but NPR-B, was added to NPR-A, the band for NPR-A was detected as a monomer (Fig. 5, Fig. S7). We applied BN-PAGE to the various ANP mutants and investigated how the locations of the mutations affect NPR-A dimerization. Focusing on the N-terminus deletion mutants of ANP, the findings of rANP [3–28] and rANP [1–28] were almost identical. In contrast, dimerization was induced in hANP [5–28] and hANP [7–28], but the bands were tailed slightly to the region of the NPR-A monomer (Fig. 5, Fig. S7). We showed that Arg4(ANP) formed a hydrogen bond with Ser6(ANP) in NPR-A complexed with hANP [1–28] (Fig. 4B) and deleting residues 4–6 in ANP led to structural instability of bound ANP, which could affect NPR-A dimerization.

Mutant hANP [5–27] with a deleted C-terminus induced dimerization, but several bands were shown to be tailed to the region of the NPR-A monomer compared with hANP [5–28]. (Fig. 5, Fig. S7). We showed

that the C-terminal residue Tyr28(ANP) played an important role in the formation of the tight NPR-A/ANP complex, and its side chain formed a hydrogen bond with ANP itself, stabilizing the ring structure of ANP (Fig. 4C). Thus, deleting Tyr28(ANP) reasonably led to a mild structural instability of bound ANP, which could affect NPR-A dimerization. Although most of the pseudo- $\beta$ -sheet forming between the NPR-A is missing from rANP [5–25], the electrophoretic profile of rANP [5–25] was almost identical to that of hANP [5–27] (Fig. 5, Fig. S7).

Met(O)<sup>12</sup>-hANP [1–28] comprises a methionine sulfoxide molecule formed through sulfur oxidation in Met12(ANP) of hANP [1–28], which inhibits its NPR-A agonistic properties [27,28]. The crystal structure complexed with hANP [1–28] (Fig. 3A–C) showed that the Met12(hANP) and Ile15(hANP) pair constituted a pseudo-two-fold symmetry as nonpolar residues at the top of the ring structure. Since methionine sulfoxide is hydrophilic, the two-fold symmetry as a pair of nonpolar amino acid residues at this location broke, and the resultant hydrophilic side chain could not fit the hydrophobic pocket (Fig. 3A–C). Therefore, dimerization was less likely to occur (Fig. 5, Fig. S7). However, unlike the NPR-A without ligand, the band was shown to have tailed slightly to the region of the NPR-A dimer (Fig. 5, Fig. S7), since Met(O)<sup>12</sup>-hANP [1–28] still possesses another pseudo-two-fold symmetry at the bottom of the ring structure. rANP [4–17, 23] lacks the important hydrophobic Leu21(ANP) residue that contributes to the pseudo-two-fold symmetry with Phe8(ANP) at the bottom of the ring structure and is known for its inability to behave as an NPR-A agonist [29]. Therefore, dimerization was less likely to have occurred (Fig. 5, Fig. S7).

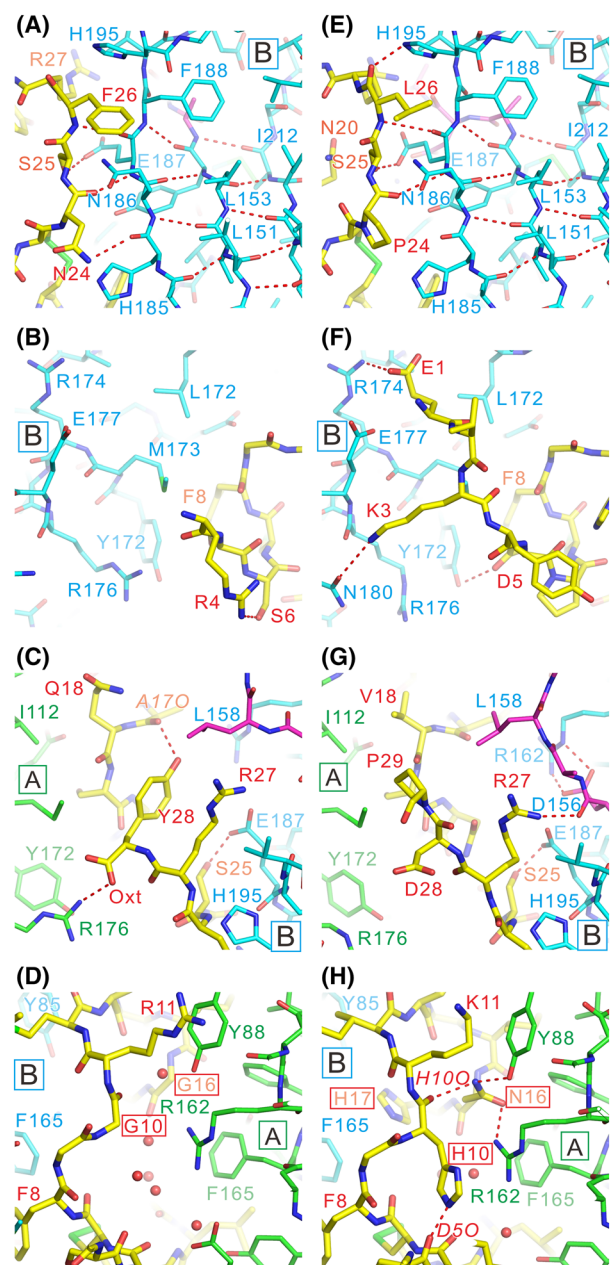


**Fig. 4.** Details of the binding of bound peptides. (A–D) Bound hANP [1–28]. (E–H) Bound DNP. Region of pseudo- $\beta$ -sheet between NPR-A and hANP [1–28] (A; the region a enclosed by the black dotted line square in Fig. 3A) or DNP (E; the region e enclosed by the black dotted line square in Fig. 3D). N-terminus region of hANP [1–28] (B; the region b enclosed by the black dotted line square in Fig. 3A) or DNP (F; the region f enclosed by the black dotted line square in Fig. 3D) before SS-bond. C-terminus region after pseudo- $\beta$ -sheet of hANP [1–28] (C; the region c enclosed by the black dotted line square in Fig. 3A) or DNP (G; the region g enclosed by the black dotted line square in Fig. 3D). Amino acid residues around DNP-specific region in hANP [1–28] (D; the region d enclosed by the black dotted line square in Fig. 3A) and DNP (H; the region h enclosed by the black dotted line square in Fig. 3D). The magenta-colored area indicates the loop 155–161 connecting the MD and MP domains (C, G; shown in magenta in Fig. 2A,B). All structure figures were prepared using PYMOL 2.4.0a (The PyMOL Molecular Graphics System, <http://www.pymol.org>).

The previous map [21] was constrained in terms of accurate modeling owing to its low resolution (Fig. S1A), despite being derived from the most superior probable interpretation. In fact, the previous model was consistent with multiple experiments, performed previously in various respects, including the relationship between ANP mutation and activity [21]. As NPR-A formed a homodimer and the facing faces of NPR-A homodimer conventionally possess a two-fold symmetry, it is reasonable to presume that the bound ANP may also have a two-fold symmetry; however, no such symmetry existed in the previous model (Fig. S1B).

Under the guidance of multiple difference density maps of distinct peptides, the present study was able to build accurate models of bound natriuretic peptides in two alternative conformations (orientations). Peptides, including the physiological ligand ANP and snake venom DNP, when bound to NPR-A, exhibited near-identical pseudo-two-fold symmetry and overall structures. The primary function of amino acid possessing a pseudo-two-fold symmetry validates the finding that these residues are essential for the hormonal activity of ANP [30]. The key difference between ANP and DNP lies in the four DNP-specific amino acid residues (His10, Asn16, His17, and Asn20) within the ring structure, which formed additional hydrogen bonds between NPR-A (Fig. 4D,H). As the corresponding residues in ANP were either small Gly or Ala, and most are also conserved in BNP and CNP (Figs 1A and 3), these small residues were considered essential for increasing the flexibility of the main chain of the peptides. Notably, sufficient space between these corresponding residues in the ANP and NPR-A was filled

## Discussion

The present study employed high-resolution structures of NPR-A with various bound natriuretic peptides possessing multiple water molecules to elucidate the NPR-A-mediated mechanism underlying substrate recognition. Intriguingly, the location of the pseudo-two-fold symmetry in the ring structure of the natriuretic peptide was discovered in a location not estimated from the primary sequence (Fig. 1A).

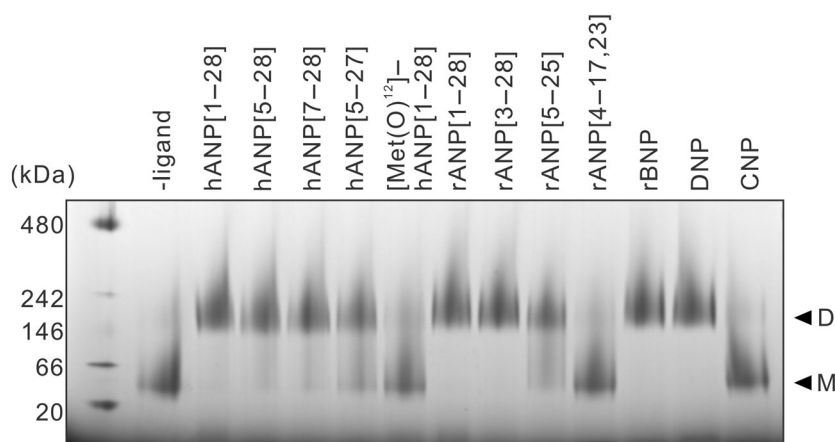


**Fig. 5.** Detection of the ligand-dependent dimerization using BN-PAGE. Following NPR-A incubation with various ligands, complexes were resolved by BN-PAGE and stained with Coomassie brilliant blue (CBB). BN-PAGE gel is from a single representative experiment, but results were reproduced in seven independent experiments ( $n = 7$ ). D, the position of NPR-A dimer; M, the position of NPR-A monomer.

with water molecules (Fig. 4D). Contrarily, the space between DNP and NPR-A was occupied by substituted His and Asn sidechains without steric hindrance, and water molecules in ANP binding were completely excluded. The substituted His and Asn form hydrogen bonds with NPR-A or DNP themselves, suggestive of crucial roles they might play in tight binding to NPR-A or in reinforcing the structure of DNP. The N-terminus of DNP had a tight interaction with NPR-A compared to that with ANP (Fig. 4B,D,F,H). Moreover, in the case of DNP, an induced fit to DNP occurred in NPR-A, resulting in a loop consisting of 155–161 of monomer B approaching DNP and forming additional hydrogen bonds (Fig. 4C,G and Fig. S5). This was not observed at all in NPR-A in the complex with ANP. Therefore, these findings suggest that DNP can bind more tightly than ANP to the NPR-A than ANP. Reports of concentration-dependent GCase activity generated by ANP or DNP in cultured cells demonstrated that the  $EC_{50}$  in the case of DNP was 10-fold higher than that for ANP [31]. Additionally, owing to enhanced stability and affinity [14,15], DNP binding could be more stable and longer-lasting than that of ANP. Consequently, DNP induced an elevated production of cGMP in comparison to ANP; this could potentially explain the functioning of DNP as a snake venom.

The pseudo-two-fold symmetry of the ring structure of ANP or DNP was deemed indispensable for NPR-A-mediated substrate recognition. In fact, rANP [4–17, 23], possessing an impaired pseudo-two-fold symmetry, revealed almost no discernible dimerization in BN-PAGE upon binding of the substrate (Fig. 5, Fig. S7). This observation prompts a query regarding the functions of the N- and C-terminus regions in the

substrates. One probable explanation indicates that they might serve as an allosteric regulator of the receptor. A previous study demonstrated that NPR-A induces rotational motion upon substrate binding [21]. In fact, the C-terminus region formed a pseudo- $\beta$ -sheet with NPR-A. Moreover, Tyr28, the C-terminal residue in ANP, assumed a crucial role in the formation of the tight NPR-A/ANP complex. The elimination of the C-terminus of the ANP triggered a reduction in the dimerization effect (Fig. 5, Fig. S7), which may be attributable to the weakening of the pseudo- $\beta$ -sheet formation in the C-terminus region that makes it difficult to maintain the exact rotation motion angle upon substrate binding. The N-terminus of ANP might assume a similar role to that of the C-terminus, as the removal of the first four N-terminal residues brings about a decrease in the dimerization effect as well (Fig. 5, Fig. S7). Currently, there is a lack of data pertaining to the role of N- and C-termini in DNP. Additionally, DNP exhibits pseudo- $\beta$ -sheet formation in the C-terminus region; moreover, the N-terminus demonstrated binding to NPR-A, which was not observed in the case of ANP (Fig. 4F). Therefore, the DNP terminus is hypothesized to functionally resemble ANP. Consequently, future experiments similar to those conducted on ANP and comparative analyses of the study outcomes with the results documented on ANP will validate the role of the N- and C-termini of DNP.

In this study, the extracellular domain of the rat NPR-A (NPR-A<sub>ECD</sub>) was investigated. Therefore, there remains a possibility that the structures of ligands bound to the extracellular domain of the rat NPR-A are apparently distinct from those in the full-length receptor. Nonetheless, the virtual resemblance of the binding constants of substrates to NPR-A<sub>ECD</sub>

to those of the full-length receptor [23], necessitates the structural determination of the full-length receptor in complex with various ligands in order to enable the thorough comprehension of the NPR-A-mediated mechanism underlying ligand recognition.

## Conclusions

The present study determined the structures of NPR-A complexed with various ligands. The bound peptides possessed pseudo-two-fold symmetry at two regions (top and bottom) in their ring structures. They played key roles in both the tight binding of the ligands to the NPR-A as well as the signal transmission mediated by the NPR-A. Kinetic and comparison studies of ANP and DNP binding to the NPR-A deepen our understanding of the ligand recognition mechanism mediated by NPR-A, which, in turn, may facilitate the development of novel agonists for the treatment of human diseases.

## Materials and methods

### Production and purification of the NPR-A<sub>ECD</sub>

Stable cell lines expressing elevated levels of the NPR-A were established according to previous methodology [24] using HEK293T cells (HEK293T:CVCL\_0063), generous gift from Yoichi Taya (National Cancer Center Research Institute, Japan). Rat NPR-A encoding cDNA (GenBank ID: NM\_012613) was purchased from OriGene Technologies Inc. (Rockville, MD, USA). Sequences, including signal sequences encoding the extracellular hormone-binding domain of the NPR-A (NPR-A<sub>ECD</sub>, amino acid residues: 1–463) were amplified by PCR using the sense and anti-sense oligonucleotide primers (underlines: restriction sites) (5′ -GGATCCCTCGAGCTAGTCTTGGTTGCAGGC-3′ and 5′ -TGCTCCACCGGTGTCTTGGTTGCAGGCTG-3′; underlined text indicates the restriction sites). Each PCR product was subcloned into the NheI and XhoI sites of a cytomegalovirus promoter-driven pIRES2-AcGFP1 vector (Clontech Laboratories Inc., Mountain View, CA, USA). HEK293T cells were co-transfected with the construct and the plasmid vector pPUR (Clontech Laboratories Inc.) using Lipofectamine 2000 (Invitrogen, Carlsbad, CA, USA). The transfected cells were selected in a growth medium containing puromycin (0.2 μg·mL<sup>-1</sup>) and cultured for 2 weeks. The top 10% of the cell population exhibiting the most intense GFP fluorescence was selected using a FACS Vantage SE cell sorter (Becton Dickinson and Co., Franklin Lakes, NJ, USA). The selected cells were cultured in a puromycin (0.2 μg·mL<sup>-1</sup>)-containing medium for 1–2 weeks, following which they were subjected to another selection cycle. Subsequently, NPR-A was purified using

affinity chromatography following a previously established methodology [21,23]. Mycoplasma was tested at the time of the stable cell line establishment. The established cell line was not authenticated.

### Crystallization, data collection, and structure determination

The following human and rat peptides were purchased from the Peptide Institute (Osaka, Japan): hANP [1–28], hANP [5–28], hANP [7–28], hANP [5–27], Met(O)<sup>12</sup>-hANP [1–28], rANP [1–28], rANP [3–28], rANP [5–25], rBNP, and hCNP. DNP was purchased from Phoenix Pharmaceuticals Inc. (Burlingame, CA, USA) and rANP [4–17, 23] from American Peptide Co. (Sunnyvale, CA, USA). The peptides hANP [1–28], hANP [7–28], hANP [5–27], rANP [1–28], DNP were used for crystallization. The NPR-A complex (10–15 mg·mL<sup>-1</sup>) and natriuretic peptides were crystallized via hanging drop vapor diffusion at room temperature with 1.2–1.6 M sodium malonate in 0.1 M MES buffer, pH 6.3–6.6. The crystals were promptly soaked in high concentrations of sodium malonate and frozen in liquid nitrogen.

Diffraction data at a wavelength of 0.9 Å were collected from crystals cooled to 100 K at BL41XU of SPring-8 using an ADSC Quantum 315 or Rayonix MX225HE CCD (charge-coupled device) detector. All data were processed using the HKL2000 program package [32]. Diffraction data from the two crystals with high resolution were averaged for each dataset. Crystal structures were determined by molecular replacement with the *apo* NPR-A (PDB ID: 1DP4) using Molrep (CCP4) [33]. Models were manually built using Coot, and atomic models were refined using CNS [34] followed by Phenix [35]. Difference Fourier maps were calculated using the CNS [34]. Structure figures were prepared using PYMOL 2.4.0a (The PyMOL Molecular Graphics System, <http://www.pymol.org>).

### Blue native polyacrylamide gel electrophoresis (BN-PAGE) analysis

NPR-A (80 pmol) was incubated with 40 pmol of peptide in 10 mL of 1× NativePAGE Sample Buffer (Thermo Fisher Scientific, Waltham, MA, USA) for 30 min at 25 °C. Samples were loaded onto 4–16% NativePAGE Bis-Tris Protein Gels (Thermo Fisher Scientific) and resolved using 1× NativePAGE Anode Buffer (Thermo Fisher Scientific) and Coomassie G-250 containing 1× NativePAGE Dark Blue Cathode Buffer containing (Thermo Fisher Scientific), in compliance with the manufacturer instructions.

### Acknowledgements

We express our sincere gratitude to Dr Chikashi Toyoshima (University of Tokyo) for supporting the

initial setup of this investigation, and to Mariko Kurakata and Kei Izumikawa (University of Tokyo) for providing technical assistance. We would like to thank K. Hasegawa and H. Okumura of the Japan Synchrotron Radiation Research Institute (JASRI) for their help in the collection of diffraction data at BL41XU of SPring-8. We would like to thank Editage ([www.editage.jp](http://www.editage.jp)) for English language editing. This study was supported by JSPS KAKENHI Grant No. JP22K19375 and JP22570110 to HO, JSPS KAKENHI Grant No. JP21K06044 to HO and MK; Platform Project for Supporting Drug Discovery and Life Science Research (Basis for Supporting Innovative Drug Discovery and Life Science Research [BINDS]) (Grant Nos. JP17am0101080, JP18am0101080, JP19am0101080, JP20am0101080) to HO; and a research grant from the Naito Science and Engineering Foundation to HO.

## Conflict of interest

The authors declare no conflict of interest.

## Author contributions

HO: conceptualization; funding acquisition; project administration; investigation; writing-original draft preparation; writing-review and editing. MK: conceptualization; funding acquisition; investigation; writing-original draft preparation; writing-review and editing.

## Peer review

The peer review history for this article is available at <https://www.webofscience.com/api/gateway/wos/peer-review/10.1111/febs.17104>.

## Data availability statement

The coordinates and structure factors for NPR-A complexed with ligands have been deposited in the Protein Data Bank (PDB) under the accession codes [7BRG](#) for rANP [1–28] complex, [7BRH](#) for hANP [1–28] complex, [7BRI](#) for DNP, [7BRJ](#) for hANP [7–28], [7BRK](#) for hANP [5–27].

## References

- de Bold AJ, Borenstein HB, Veress AT & Sonnenberg H (1981) A rapid and potent natriuretic response to intravenous injection of atrial myocardial extract in rats. *Life Sci* **28**, 89–94.
- Currie MG, Geller DM, Cole BR, Boylan JG, YuSheng W, Holmberg SW & Needleman P (1983) Bioactive cardiac substances: potent vasorelaxant activity in mammalian atria. *Science* **221**, 71–73.
- Grammer RT, Fukumi H, Inagami T & Misono KS (1983) Rat atrial natriuretic factor. Purification and vasorelaxant activity. *Biochem Biophys Res Commun* **116**, 696–703.
- Atarashi K, Francosaenz R & Mulrow PJ (1984) Inhibition of aldosterone production by atrial natriuretic peptides. *Clin Res* **32**, A785.
- Kangawa K & Matsuo H (1984) Purification and complete amino acid sequence of alpha-human atrial natriuretic polypeptide (alpha-hANP). *Biochem Biophys Res Commun* **118**, 131–139.
- Sudoh T, Kangawa K, Minamino N & Matsuo H (1988) A new natriuretic peptide in porcine brain. *Nature* **332**, 78–81.
- Sudoh T, Minamino N, Kangawa K & Matsuo H (1990) C-type natriuretic peptide (CNP): a new member of natriuretic peptide family identified in porcine brain. *Biochem Biophys Res Commun* **168**, 863–870.
- Nakao K, Ogawa Y, Suga S & Imura H (1992) Molecular biology and biochemistry of the natriuretic peptide system. I: Natriuretic peptides. *J Hypertens* **10**, 907–912.
- Koller KJ, Lowe DG, Bennett GL, Minamino N, Kangawa K, Matsuo H & Goeddel DV (1991) Selective activation of the B natriuretic peptide receptor by C-type natriuretic peptide (CNP). *Science* **252**, 120–123.
- Chusho H, Tamura N, Ogawa Y, Yasoda A, Suda M, Miyazawa T, Nakamura K, Nakao K, Kurihara T, Komatsu Y *et al.* (2001) Dwarfism and early death in mice lacking C-type natriuretic peptide. *Proc Natl Acad Sci USA* **98**, 4016–4021.
- Schweitz H, Vigne P, Moinier D, Frelin C & Lazdunski M (1992) A new member of the natriuretic peptide family is present in the venom of the green mamba (*Dendroaspis angusticeps*). *J Biol Chem* **267**, 13928–13932.
- Lisy O, Jougasaki M, Heublein DM, Schirger JA, Chen HH, Wennberg PW & Burnett JC (1999) Renal actions of synthetic dendroaspis natriuretic peptide. *Kidney Int* **56**, 502–508.
- Best PJ, Burnett JC, Wilson SH, Holmes DR Jr & Lerman A (2002) Dendroaspis natriuretic peptide relaxes isolated human arteries and veins. *Cardiovasc Res* **55**, 375–384.
- Singh G, Kuc RE, Maguire JJ, Fidock M & Davenport AP (2006) Novel snake venom ligand dendroaspis natriuretic peptide is selective for natriuretic peptide receptor-a in human heart: downregulation of natriuretic peptide receptor-a in heart failure. *Circ Res* **99**, 183–190.

- 15 Chen HH, Lainchbury JG & Burnett JC Jr (2002) Natriuretic peptide receptors and neutral endopeptidase in mediating the renal actions of a new therapeutic synthetic natriuretic peptide dendroaspis natriuretic peptide. *J Am Coll Cardiol* **40**, 1186–1191.
- 16 Lisy O, Huntley BK, McCormick DJ, Kurlansky PA & Burnett JC Jr (2008) Design, synthesis, and actions of a novel chimeric natriuretic peptide: CD-NP. *J Am Coll Cardiol* **52**, 60–68.
- 17 Lee CY, Huntley BK, McCormick DJ, Ichiki T, Sangaralingham SJ, Lisy O & Burnett JC Jr (2016) Cenderitide: structural requirements for the creation of a novel dual particulate guanylyl cyclase receptor agonist with renal-enhancing in vivo and ex vivo actions. *Eur Heart J Cardiovasc Pharmacother* **2**, 98–105.
- 18 Chinkers M, Garbers DL, Chang MS, Lowe DG, Chin HM, Goeddel DV & Schulz S (1989) A membrane form of guanylate cyclase is an atrial natriuretic peptide receptor. *Nature* **338**, 78–83.
- 19 Garbers DL, Chrisman TD, Wiegand P, Katafuchi T, Albanesi JP, Bielinski V, Barylko B, Redfield MM & Burnett JC Jr (2006) Membrane guanylyl cyclase receptors: an update. *Trends Endocrinol Metab* **17**, 251–258.
- 20 Potter LR (2011) Guanylyl cyclase structure, function and regulation. *Cell Signal* **23**, 1921–1926.
- 21 Ogawa H, Qiu Y, Ogata CM & Misono KS (2004) Crystal structure of hormone-bound atrial natriuretic peptide receptor extracellular domain: rotation mechanism for transmembrane signal transduction. *J Biol Chem* **279**, 28625–28631.
- 22 van den Akker F, Zhang X, Miyagi M, Huo X, Misono KS & Yee VC (2000) Structure of the dimerized hormone-binding domain of a guanylyl-cyclase-coupled receptor. *Nature* **406**, 101–104.
- 23 Misono KS, Sivasubramanian N, Berkner K & Zhang X (1999) Expression and purification of the extracellular ligand-binding domain of the atrial natriuretic peptide (ANP) receptor: monovalent binding with ANP induces 2:2 complexes. *Biochemistry* **38**, 516–523.
- 24 Okamoto N, Ogawa H & Toyoshima C (2012) A new method for establishing stable cell lines and its use for large-scale production of human guanylyl cyclase-B receptor and of the extracellular domain. *Biochem Biophys Res Commun* **426**, 260–265.
- 25 Misono KS (2000) Atrial natriuretic factor binding to its receptor is dependent on chloride concentration: a possible feedback-control mechanism in renal salt regulation. *Circ Res* **86**, 1135–1139.
- 26 Ogawa H, Qiu Y, Philo JS, Arakawa T, Ogata CM & Misono KS (2010) Reversibly bound chloride in the atrial natriuretic peptide receptor hormone-binding domain: possible allosteric regulation and a conserved structural motif for the chloride-binding site. *Protein Sci* **19**, 544–557.
- 27 Willenbrock RC, Tremblay J, Garcia R & Hamet P (1989) Dissociation of natriuresis and diuresis and heterogeneity of the effector system of atrial natriuretic factor in rats. *J Clin Invest* **83**, 482–489.
- 28 Koyama S, Terai T, Inoue T, Inomata K, Tamura K, Kobayashi Y, Kyogoku Y & Kobayashi M (1992) An oxidized analog of alpha-human atrial natriuretic polypeptide is a selective agonist for the atrial-natriuretic-polypeptide clearance receptor which lacks a guanylate-cyclase. *Eur J Biochem* **203**, 425–432.
- 29 Maack T, Suzuki M, Almeida FA, Nussenzveig D, Scarborough RM, McEnroe GA & Lewicki JA (1987) Physiological role of silent receptors of atrial natriuretic factor. *Science* **238**, 675–678.
- 30 Bovy PR (1990) Structure activity in the atrial natriuretic peptide (Anp) family. *Med Res Rev* **10**, 115–142.
- 31 Johns DG, Ao ZH, Heidrich BJ, Hunsberger GE, Graham T, Payne L, Elshourbagy N, Lu Q, Aiyar N & Douglas SA (2007) Dendroaspis natriuretic peptide binds to the natriuretic peptide clearance receptor. *Biochem Biophys Res Commun* **358**, 145–149.
- 32 Otwinowski Z & Minor W (1997) Processing of X-ray diffraction data collected in oscillation mode. *Methods Enzymol* **276**, 307–326.
- 33 Vagin A & Teplyakov A (1997) MOLREP: an automated program for molecular replacement. *J Appl Crystallogr* **30**, 1022–1025.
- 34 Brünger AT, Adams PD, Clore GM, DeLano WL, Gros P, Grosse-Kunstleve RW, Jiang JS, Kuszewski J, Nilges M, Pannu NS *et al.* (1998) Crystallography & NMR system: a new software suite for macromolecular structure determination. *Acta Crystallogr D* **54**, 905–921.
- 35 Liebschner D, Afonine PV, Baker ML, Bunkoczi G, Chen VB, Croll TI, Hintze B, Hung LW, Jain S, McCoy AJ *et al.* (2019) Macromolecular structure determination using X-rays, neutrons and electrons: recent developments in Phenix. *Acta Crystallogr D Struct Biol* **75**, 861–877.

## Supporting information

Additional supporting information may be found online in the Supporting Information section at the end of the article.

**Fig. S1.** Comparison of the ANP ring structure and maps.

**Fig. S2.** Comparison of the DNP ring structure and maps.

**Fig. S3.**  $|F_{\text{obs}}| - |F_{\text{calc}}|$  electron density maps around the bound peptides.

**Fig. S4.**  $|F_{\text{obs}}| + |F_{\text{calc}}|$  electron density maps around the bound peptides.

**Fig. S5.** Structures of the bound peptides.

**Fig. S6.** Pseudo-two-fold regions of bound peptides.

**Fig. S7.** Detection of the ligand-dependent dimerization using BN-PAGE.